Tuning the ferroelectric properties of trialkylbenzene-1,3,5-tricarboxamide (BTA)

ADVANCED ELECTRONIC MATERIALS
www.advelectronicmat.de

Tuning the Ferroelectric Properties of Trialkylbenzene-1,3,5-tricarboxamide (BTA)

*Indre Urbanaviciute, Xiao Meng, Tim D. Cornelissen, Andrey V. Gorbunov, Subham Bhattacharjee, Rint P. Sijbesma, and Martijn Kemerink**

This study demonstrates how simple structural modification of a prototypical organic ferroelectric molecule can be used to tune its key ferroelectric properties. In particular, it is found that shortening the alkyl chain length of trialkylbenzene-1,3,5-tricarboxamide (BTA) from $C_{18}H_{37}$ to C_6H_{13} causes an increase in depolarization activation energy (≈1.1–1.55 eV), coercive field (≈25–40 V μm^{-1}), and remnant polarization (≈20–70 mC m^{-2}). As the polarization enhancement far exceeds the geometrically expected factor, these observations are attributed to an increase in the intercolumnar interaction. The combination of the mentioned characteristics results in a record polarization retention time of close to three months at room temperature for capacitor devices of the material having the shortest alkyl chain. The long retention and the remnant polarization that is as high as that of P(VDF:TrFE) distinguish the BTA-C6 material from other small molecular organic ferroelectrics and make it a perspective choice for applications that require cheap, flexible, and lightweight ferroelectrics.

Organic materials for electronic applications come with a well-known package of beautiful properties like cheap and easy processing, flexibility, lightness, low environmental impact, etc. Their key asset though lies in the versatility of the organic synthesis, which allows broad variations in molecular structure and elemental composition. This capability of organic synthesis has been fruitfully exploited in the fields of conductors, semiconductors, and insulators. The field of organic ferroelectrics has started to gain interest only recently, even though the first truly organic ferroelectric was announced in 1956.[1] For a general overview of the multitude of possible ferroelectric mechanisms in organic matter we refer to the review papers of Horiuchi and Tokura and Tayi et al.[2,3] One of the most used and possibly the most convenient approach to achieve ferroelectricity in a molecular system is through the introduction of free-to-rotate dipolar segments ($-CH_2-CF_2-$, amide, urea, etc.); in many cases this leads to ferroelectric behavior at room temperature.[4] In this manner, ferroelectricity has been established in ferroelectric polymers, such as P(VDF:TrFE) or odd-numbered nylons.[5,6] Weak noncovalent interactions, ordinarily present in organic substances, further assure long-range order among dipolar units and thereby facilitate collective rotation of the dipolar moieties upon bias, resulting in a field-reversible bulk polarization that stays even in the absence of an applied electric field.

The properties mentioned above are not restricted to the polymer materials; for example, small molecular weight liquid crystals, containing switchable dipolar groups, also show ferroelectric behavior.[7–14] Ferroelectric liquid crystals, especially of columnar type, have several important advantages compared to ferroelectric polymers. First, these bent-core, disc- and umbrella-shaped molecules tend to self-assemble into columnar hexagonal manner.[3,15,16] It has been speculated that in this conformation the separate columns could be used as single memory bits which would allow fabrication of ultrahigh-density memory devices.[8,17] For more short-term applications self-assembly improves order in the system and thereby device characteristics. Also, columnar discotic liquid crystals are very sensitive to changes in the molecular structure, which makes for an ideal handle to steer their characteristics.[8,18–21]

Organic molecules with liquid crystalline properties typically consist of a functional core and surrounding soluble flexible tails. Changing the length of these peripheral chains is an uncomplicated, easily implementable structural variation. Being insulating, these structurally simple (e.g., $-CH_2-CH_2-CH_3$) tails usually do not possess any other function than physical separation of the active molecular parts or enhancement of solubility and liquid crystallinity.[19,22,23] Despite that, they may have a surprisingly big effect on the functional properties

I. Urbanaviciute, T. D. Cornelissen, Prof. M. Kemerink
Complex Materials and Devices
Department of Physics, Chemistry and Biology (IFM)
Linköping University
58183 Linköping, Sweden
E-mail: martijn.kemerink@liu.se

X. Meng, Dr. S. Bhattacharjee, Prof. R. P. Sijbesma
Laboratory of Macromolecular and Organic Chemistry
Eindhoven University of Technology
P.O. Box 513, 5600 MB, Eindhoven, The Netherlands

A. V. Gorbunov
Department of Applied Physics
Eindhoven University of Technology
P.O. Box 513, 5600 MB, Eindhoven, The Netherlands

The ORCID identification number(s) for the author(s) of this article can be found under https://doi.org/10.1002/aelm.201600530.

DOI: 10.1002/aelm.201600530

of the material. The issue of flexible chain length in defining material characteristics has been discussed multiple times for semiconducting and/or supramolecular materials.[22,24–26] However, comparatively few works have addressed structure–property relations of molecular ferroelectrics in a systematic manner.[8,19,27] One of the few studies focusing on proper organic ferroelectric materials is by Kishikawa et al., who probed ferroelectric columnar hexagonal liquid crystalline urea with C_4H_9 to $C_{16}H_{33}$ long alkyl chains.[28] The observed inverse proportionality between alkyl chain length and remnant polarization value was explained to rely on the geometrical filling alone.

The molecule we use for our studies is the well-known columnar liquid crystal trialkylbenzene-1,3,5-tricarboxamide (BTA).[29,30] It has a π-stacking benzene core, three hydrogen-bonding dipolar amide groups, and peripheral flexible alkyl chains for enhancement of solubility and liquid crystallinity (**Figure 1**a). Initially BTA has attracted a lot of interest due to structure-related strong intermolecular interaction and the resultant formation of supramolecular polymers in solution, the ability to create gels as well as rigid nanofibers.[31–34] The ferroelectric behavior, however, is a relatively new finding.[9,35] Fitié et al. were first to probe BTA homologues with 18, 10, and 6 carbons-long alkyl chain (BTA-C18, BTA-C10, and BTA-C6). While BTA-C18 and BTA-C10 were successfully functioning as ferroelectrics in a columnar hexagonal liquid crystalline phase (Figure 1b), BTA-C6, however, showed no ferroelectric switching in liquid crystal cell devices.[36] Gorbunov et al. further studied thin spin-coated BTA-C10 and BTA-C18 films and proved the true ferroelectric nature of the material,[35] which had been predicted in previous theoretical works on BTAs[37–40] and on dipolar discotic particles in general.[41–44] This is further discussed in the Supporting Information.

Here, we systematically pursue tuning of the ferroelectric properties of the prototypical molecular ferroelectric BTA. In contrast to the results from ref. [28], our material shows polarization enhancement with decreasing alkyl chain length, exceeding the geometrical filling factor. Also the activation energy and rate of depolarization, the coercive field and the relevant phase transition temperatures are all found to be almost continuously tunable with peripheral tail length. The concerted effect of these factors leads, for optimal—shortest—chain length, to a record material with performance that is comparable to that of the P(VDF:TrFE).

Five BTA homologues BTA-C6, C8, C10, C12, and C18 (Figure 1a) have been synthesized using a standard method as described in the Supporting Information and ref. [36]. First, we probe the thermal properties of all BTA compounds using differential scanning calorimetry (DSC). DSC curves (Figure S1 of the Supporting Information) have two characteristic peaks, representing crystalline-to-liquid crystalline and liquid crystalline-to-isotropic phase transitions.[45,46] Collective switching of amide groups is only possible close to the liquid-crystalline phase. Deep in the low temperature crystalline phase the coercive field becomes unattainably high, possibly above the breakdown limit due to reduced molecular mobility; above the melting temperature the material is paraelectric.[35] Therefore, the phase diagram gives the essential information about the operational temperature window of the devices. The DSC trace peak positions for cooling are summarized in Figure 1c. Additional data points for the BTA-C14 molecule, reported by Shishido et al., are indicated as asterisks in Figure 1c.[47] A clear linear trend with decreasing alkyl chain length from 18 to 10 carbons is visible as broadening of the temperature range over which ferroelectric behavior is to be expected. The change in trend found for the short-tailed BTA-C6 and BTA-C8 may be explained by changes in the alkyl chain conformation due to shortness.[46] However, the effect disappears if the benzene core is changed for a nonconjugated cyclohexane lacking π–π interactions.[45]

To examine temperature-related changes in molecular packing we performed temperature scans of wide angle X-ray scattering (WAXS) of powdered BTA samples (Figure S2, Supporting Information). Rearrangement of the molecules is reflected in the changed diffraction pattern upon Cr-LC and

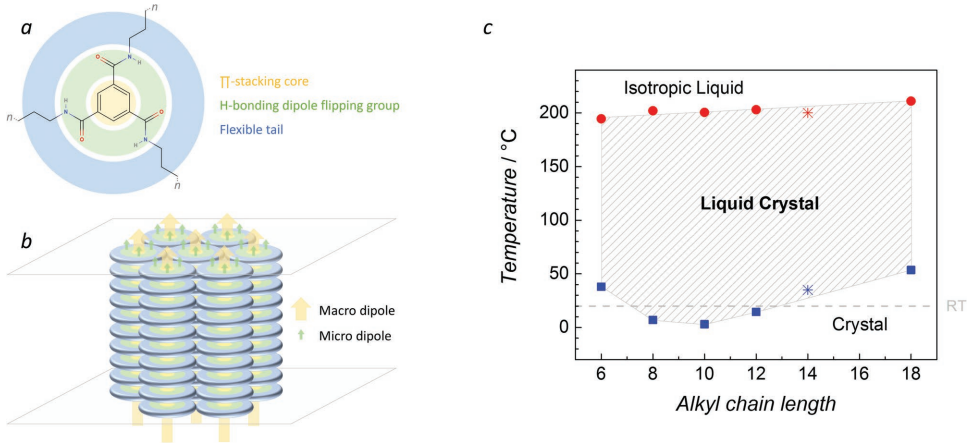

Figure 1. a) A chemical structure of discotic BTAs ($n = 6, 8, 10, 12, 18$, corresponding to the alkyl chain C_nH_{n+1}) and b) Columnar hexagonal packing resulting in a molecular macrodipole and ferroelectric behavior in a prepared device. c) Phase transition temperatures for BTA molecules with different alkyl chain lengths. Red circles represent melting point, which is ≈200 °C irrespective of the alkyl chain length; blue squares are crystal-to-liquid crystal transition temperatures: 38 °C for BTA-C6, 7 °C for BTA-C8, 3 °C for BTA-C10, 14.5 °C for BTA-C12, and 53.5 °C for BTA-C18. Asterisks are data measured by Shishido et al.[47] The shaded liquid crystalline phase is ferroelectric.[35] BTA-C6, C8, C10, and C12 material devices successfully operate at room temperature.

LC-I phase transitions. A characteristic diffraction peak spacing ratio of 1:√3:2 in the reciprocal q-space further discloses the hexagonal packing character of the molecules in the LC phase, which is considered to be a prerequisite for ferroelectric activity.[35,36] Phase transition temperatures obtained here match the values measured by the DSC (Figure S1b, Supporting Information).

For potential application purposes it is important that, for the shortest chain lengths, the LC phase that supports ferroelectricity extends down to room temperature and even slightly below. Even though BTA-C6 undergoes the Cr-LC phase transition above room temperature at ≈38 °C, the ferroelectric response is still observed inside the pretransitional "soft" crystalline state. This is most likely due to the short alkyl chains that, differently to the BTA-C18 case, do not form a bulky crystalline structure and do not prevent the amide flipping. To illustrate this effect we perform a temperature scan of polarization hysteresis loops on metal/ferroelectric/metal devices, see Figure S3 (Supporting Information). For details of the device fabrication and measurement procedure we refer to the Supporting Information. The results show excellent stability of the remnant polarization in the whole temperature range from 80 °C down to room temperature ≈20 °C for all materials with the exception of BTA-C18, which enters the crystalline phase ≈50 °C and becomes nonswitchable. The extracted coercive field dependence on temperature (Figure S3e,f, Supporting Information) obeys the theory for thermally activated nucleation limited switching by Vopsaroiu et al.[48] More details on this theory can be found in the Supporting Information. There is a change in a slope exactly at the phase transition temperature for BTA-C6 and BTA-C18. However, BTA-C18 experiences a drastic polarization drop and further behaves as a simple dielectric. No change in the slope was observed for BTA-C8, BTA-C10, and BTA-C12 due to absence of phase transitions within the measured temperature range.

As cast from solution, BTA self-arranges into hexagonally packed long columns in-plane to the substrate (clearly seen in AFM images, Figure S8, Supporting Information). To operate out-of-plane devices we need to break the initial structure and field-align the molecules homeotropically. Varying alignment levels cause remnant polarization variations up to ≈30% among devices. We choose devices with the closest to the ideal homeotropic alignment, i.e., the highest saturated remnant polarization values, for further parameter comparison. P–E curves with the maximum experimentally achieved remnant polarization at different comfortable measurement conditions, as specified in the caption, are given for all materials in **Figure 2**a. An obvious increasing trend in remnant polarization is seen with shortening the peripheral tails (Figure 2b): 67 mC m^{-2} for BTA-C6, 48 mC m^{-2} for BTA-C8, 45 mC m^{-2} for BTA-C10, 31 mC m^{-2} for BTA-C12, and 21 mC m^{-2} for BTA-C18.

To understand this trend, we calculate the theoretical polarization value P of a perfectly packed hexagonal lattice as a reference, using $P = M/V$, where $M = N\sum\mu_0$ is the total dipole moment from N molecules and V is the device volume. For this, we assume that the dipole moment per molecule μ_0 is constant, i.e., independent of the intercolumnar distance. The calculated values therefore only reflect the geometric filling factor. A value of $\mu_0 = 12$ D $\approx 4 \times 10^{-29}$ C m is chosen to fit the polarization of BTA-C18 as a reference point, which is also an upper limit of the theoretical estimates of μ_0.[37,49] The molecular packing parameters for calculations are obtained from WAXS measurements (Figure S3, Supporting Information), giving an intercolumnar distance of 1.62 nm for BTA-C6, 1.94 nm for BTA-C10, 2.08 nm for BTA-C12, and 2.5 nm for BTA-C18; a relative comparison of these measures is shown in the inset of Figure 2b. The intercolumnar distances for the other homologues have been extrapolated from an expected linear trend.[45] The intermolecular distance within a column, determined by the length of the N—H···O hydrogen bond, is the same $c = 0.34$ nm for all materials.

Surprisingly, the experimental remnant polarization versus chain length curve does not match the calculations (solid line), as seen in Figure 2b. For shorter chains the polarization exceeds the calculated numbers significantly and follows a superlinear trend, which shows that additional effects on top of the geometric filling are at play. As ionic input, electrochemical reactions and the effect of different dead layers can be discarded as improbable (see the Supporting Information), we speculate that this nonlinear polarization enhancement is

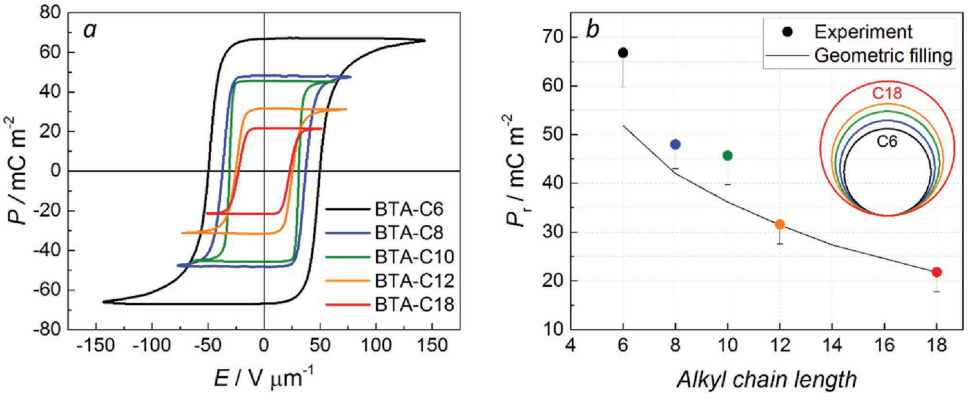

Figure 2. a) Polarization hysteresis loops at optimal conditions for all BTA materials. Measurement temperature 50 °C for BTA-C6, 55 °C for BTA-C8, 70 °C for BTA-C10 and BTA-C12, 100 °C for BTA-C18, applied field frequency 5–10 Hz. b) Remnant polarization versus alkyl chain length. Symbols are the maximum experimental remnant polarization values observed with a variation range among 5 devices with the highest parameters to show reproducibility. The line indicates expectation on basis of geometrical filling with a constant dipole moment per molecule $\mu_0 = 12$ D. Inset: relative column diameters at 80 °C as based on the intercolumnar distances measured by WAXS.

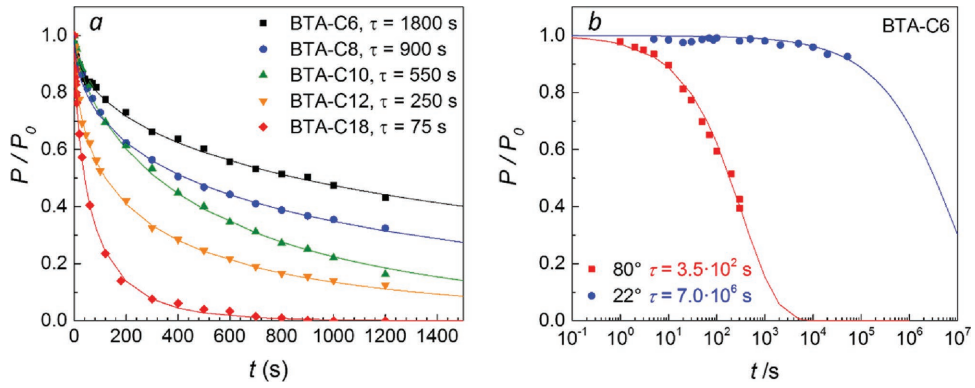

Figure 3. a) Polarization retention of BTA capacitor devices at 70 °C. Lines are stretched exponential fits with a stretching exponent $\beta = 0.5$–0.65 and time constant τ given in the legend. b) Retention for an Al/BTA-C6/Al capacitor device at 80 and 22 °C. The time constants obtained from fitting a stretched exponential are shown in the legend.

related to a cooperative effect among columnar macrodipoles. The assumption is made based on a similar effect among microdipoles within columns, which has been predicted for BTA stacks using density functional theory (DFT) and molecular dynamics (MD) computations performed by Albuquerque et al. and Kulkarni et al. This implies that the dipole moment per column increases due to enhanced intercolumnar interactions, similar to the enhancement of the molecular dipole upon lengthening of the BTA column.[37–40,49] Naturally, the effect is more pronounced in tighter packed systems. Further discussion can be found in the Supporting Information. Theoretical modeling of the underlying processes is ongoing and will be published in a separate paper.

As seen in Figure 4b, the average coercive field obtained from measurements on multiple devices at 70 °C and 5 Hz frequency has a clear increasing trend with shortening of the alkyl chain, too: ≈25, ≈30, ≈32, ≈37, and ≈42 V μm^{-1} for BTA-C18, C12, C10, C8, and C6, respectively. Minor variation of the value among devices is most likely caused by slight differences in saturation polarization, thickness of the spin-coated film and dead layers. The coercive field values for BTA-C18 and BTA-C10 obtained by Fitié et al. are marked as asterisks and match the current results. As the polarization switching process in BTAs is nucleation-limited,[35] the coercive field value corresponds to the energy barrier for nucleation of the critical size domains (see Equation (S1) of the Supporting Information).[48] Further, following the adapted Landau–Devonshire theory, this energy barrier is directly proportional to the volume of the critical domain and the polarization squared.[48] Naturally, this leads to a higher coercive field for materials with higher remnant polarization values and higher layer order. Later we show that both these characteristics correspond to the molecules with the shorter alkyl chains.

We anticipated that the high remnant polarization and coercive field together with the previously proposed stronger intercolumnar interaction would also correspond to increased depolarization activation energy and improved data retention for shorter-substituted molecules. Therefore, we performed direct electrical polarization relaxation measurements on metal/ferroelectric/metal devices at different temperatures.[50] As an example, the polarization decay for all materials at 70 °C is shown in **Figure 3**a; a full data set can be found in Figure S5 (Supporting Information). Indeed, Figure 3a clearly shows enhanced retention with changing the alkyl chain length from 18 to 6 carbon atoms. The polarization decay was fitted with a stretched exponential function ~exp[$-(t/\tau)^{\beta}$] with $\beta \approx 0.5$, which is a typical expression to describe decay processes over a (random) energy barrier and is widely used for relaxation analysis in disordered systems that have a distribution of relaxation times.[51,52] From the temperature dependence of the resulting time constants τ, the depolarization activation energy W_b was then obtained by fitting to a simple Arrhenius equation (Figure S4, Supporting Information). The results are shown in **Figure 4**c. Previously, Fitié et al. reported the depolarization activation energy for liquid crystal cell devices of BTA-C18 and

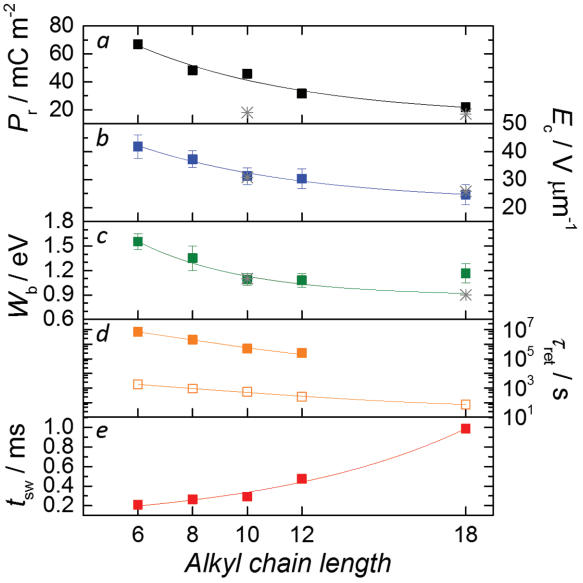

Figure 4. Trends in the experimentally observed ferroelectric properties versus alkyl chain length of the BTA materials. a) Maximum saturated remnant polarization. b) Coercive field at 70 °C and 5 Hz probe frequency. c) Depolarization activation energy. d) Polarization retention time constant τ_{ret} at room temperature (full squares) and 70 °C (hollow squares) plotted using semilogarithmic scale. e) Switching time t_{sw} at 80 °C and 50 V μm^{-1} applied field. Asterisks represent data taken from literature.[36] Lines are guides to the eye.

BTA-C10 to be 0.9 and 1.1 eV, respectively.[9] These data are marked as asterisks in Figure 4c for reference. Our results show that this energy barrier continuously increases from ≈1.1 eV for BTA-C18 to ≈1.55 eV for BTA-C6. The extracted W_b parameter here may be considered as a barrier for nucleation, although it should be kept in mind that it also reflects a property of a whole device, including electrodes and possible depolarization fields arising from, e.g., "dead" interface layers.[35,48,51,53] However, the observed significant changes in W_b for shorter alkyl chain lengths are unlikely to be driven by the difference in the depolarization field only.

As expected, the higher W_b for BTA-C6 is well in line with the trends observed for P_r and E_c as shown in panels (a–c) of Figure 4. Using the remnant polarization and coercive field values, we can fit the energy barrier W_b to the thermally activated nucleation limited switching formalism, Equation (S1) (Supporting Information).[48] Keeping the attempt frequency equal to the amide rotation frequency ν_0 = 15.7 THz,[40] this gives an increasing critical domain size from 10 nm^3 (6 molecules) for BTA-C18 to 39 nm^3 (56 molecules) for BTA-C6. Greater critical domain sizes, i.e., longer column lengths, denote higher order for shorter-substituted homologues, which, as discussed previously and will be shown later, has a positive impact on other characteristics.

An important consequence of the high depolarization activation energy is that it results in a remarkable increase of the polarization retention time, especially at lower temperatures. As shown in Figure 3b, for BTA-C6 the time constant of the polarization decay increases from ≈6 min at 80 °C to 7 × 10^6 s at room temperature, which is more than 80 days. To compare, the same parameter for BTA-C8 is ≈2 × 10^6 s, BTA-C10 ≈5 × 10^5 s, and BTA-C12 ≈2.5 × 10^5 s (Figure S5, Supporting Information). BTA-C18 is nonswitchable at room temperature. The retention time at room temperature and at 70 °C is plotted in Figure 4d for all materials and shows an exponential growth with shorter tails, which corresponds to the thermal activation over the growing energy barrier. In fact, BTA-C6 holds a retention record not only among BTAs, but also has one of the highest results reported for organic small molecule ferroelectrics.[8,14,54]

Another pleasant feature of the BTA devices is the submillisecond polarization switching time (Figure S12, Supporting Information, and ref. [35]). It might be expected that the increasing coercive field, remnant polarization, and depolarization activation energy with decreasing alkyl chain length would be accompanied by an increased switching time.[48] The latter would be undesired from an application perspective. Fortunately, the experimental results summarized in Figure 4e show that the polarization switching time decreases with shorter tail from 0.98 ms for BTA-C18 to 0.2 ms for BTA-C6 at 80 °C. This counterintuitive observation can be rationalized by taking the influence of disorder in the system into account. Previously we elucidated that the polarization switching process in BTAs is nucleation-limited and highly dispersive with a broad log-normal distribution of switching times.[35,55,56] The effect of disorder, corresponding to the wider switching time distribution, was more significant for BTA-C18 compared to BTA-C10.[35] The grazing-incidence WAXS (GIWAXS) measurement results for BTA-C10 and BTA-C18 also evinced the disordered nature of the materials, especially those having long alkyl chains.[50] More evidence for increasing order with shorter side chains discloses if we fit the experimental switching time using the Vopsaroiu theory (Equation (S2), Supporting Information) with the experimental values of the energy barrier, remnant polarization, and coercive field, keeping the attempt frequency constant at ν_0 = 15.7 THz. The extracted critical domain size grows from 15 to 60 molecules, comparing BTA-C18 and BTA-C6. On the basis of these results, we attribute the high polarization switching speed of shorter-substituted molecules to a higher packing order. Altogether this is consistent with the proposed effect of the higher coupling among columnar macrodipoles due to shorter spatial separation of formed molecular stacks.

To further demonstrate the application potential of BTA-C6 devices, we measured the electrical fatigue in air at 45 °C and a slow 1 Hz field sweeping rate. After 10^5 cycles the polarization decreased by a factor two as compared to the initial value (Figure S13, Supporting Information). Together with the remnant polarization, coercive field, polarization switching time, and data retention being already comparable to the performance of P(VDF:TrFE) thin film devices,[57–61] this makes BTA-C6 interesting not only from a scientific, but also from an application point of view.

We have shown that the ferroelectric properties of an organic discotic small molecule BTA (benzene-1,3,5-tricarboxamide) can be tuned by changing the length of peripheral alkyl chains. These flexible tails influence molecular packing by determining the intercolumnar distance in a columnar hexagonal liquid crystalline phase. Therefore, the shorter tails not only increase the dipole density, but also result in stronger interaction among columnar macrodipoles. This augments remnant polarization, coercive field, depolarization activation energy, and improves polarization retention. We have observed experimentally that the change of the alkyl chain length from 18 to 6 carbon atoms leads to a remnant polarization boost from 20 mC m^{-2} for BTA-C18 to almost 70 mC m^{-2} for BTA-C6, which fails to be explained by simple geometrical filling. Furthermore, the coercive field has almost doubled from ≈25 to ≈40 V μm^{-1} (T = 70 °C, f = 5 Hz) for BTA-C18 and BTA-C6, respectively. The depolarization activation energy has also increased from ≈1 eV for BTA-C18 to ≈1.55 eV for BTA-C6. As a result, the polarization retention for BTA-C6 has become close to three months (≈80 days) at room temperature, which is incomparably better than several minutes registered for BTA-C18. This achievement is also facilitated by the fact that the temperature range of the ferroelectric phase extends to room temperature and below for shorter-substituted homologues, as compared to >50 °C for BTA-C18.

The excellent tunability of the ferroelectric properties of the prototypical BTA material can potentially be applied to the whole class of discotic columnar liquid crystalline materials. The study results may be taken as an example how systematic molecular engineering can lead us toward high-quality devices: regarding its ferroelectric properties, the BTA-C6 material sits in the same class as the commercially available ferroelectric polymer P(VDF:TrFE) and with the record retention time it can compete with the best reported organic ferroelectric materials to date.

Supporting Information

Supporting Information is available from the Wiley Online Library or from the author.

Acknowledgements

The work of A.V.G. was supported by the NWO Nano program. I.U. acknowledges funding by Vetenskapsrådet. T.D.C. acknowledges financial support from the Swedish Government Strategic Research Area in Materials Science on Functional Materials at the Linköping University (Faculty Grant SFO Mat LiU No. 2009 00971).

Conflict of Interest

The authors declare no conflict of interest.

Keywords

alkyl chains, benzene-1,3,5-tricarboxamide, ferroelectric memories, organic ferroelectrics, polarization retention

Received: December 8, 2016
Revised: March 29, 2017
Published online: May 16, 2017

[1] A. L. Solomon, *Phys. Rev.* **1956**, *104*, 1191.
[2] S. Horiuchi, Y. Tokura, *Nat. Mater.* **2008**, *7*, 357.
[3] A. S. Tayi, A. Kaeser, M. Matsumoto, T. Aida, S. I. Stupp, *Nat. Chem.* **2015**, *7*, 281.
[4] S. Fujisaki, H. Ishiwara, Y. Fujisaki, *Appl. Phys. Lett.* **2007**, *90*, 162902.
[5] T. Yamada, *J. Appl. Phys.* **1981**, *52*, 6859.
[6] J. I. Scheinbeim, J. W. Lee, B. A. Newman, *Macromolecules* **1992**, *25*, 3729.
[7] K. Kishikawa, S. Nakahara, Y. Nishikawa, S. Kohmoto, M. Yamamoto, *J. Am. Chem. Soc.* **2005**, *127*, 2565.
[8] D. Miyajima, F. Araoka, H. Takezoe, J. Kim, K. Kato, M. Takata, T. Aida, *Science* **2012**, *336*, 209.
[9] C. F. C. Fitié, W. S. C. Roelofs, M. Kemerink, R. P. Sijbesma, *J. Am. Chem. Soc.* **2010**, *132*, 6892.
[10] J. Guilleme, E. Cavero, T. Sierra, J. Ortega, C. L. Folcia, J. Etxebarria, T. Torres, D. González-Rodríguez, *Adv. Mater.* **2015**, *27*, 4280.
[11] S. Kang, X. Li, S. Kawauchi, M. Tokita, J. Watanabe, *Mol. Cryst. Liq. Cryst.* **2011**, *549*, 184.
[12] G. Dantlgraber, A. Eremin, S. Diele, A. Hauser, H. Kresse, G. Pelzl, C. Tschierske, *Angew. Chem. Int. Ed.* **2002**, *41*, 2408.
[13] D. Krüerke, P. Rudquist, S. T. Lagerwall, H. Sawade, G. Heppke, *Ferroelectrics* **2000**, *243*, 207.
[14] Y. Okada, S. Matsumoto, Y. Takanishi, K. Ishikawa, S. Nakahara, K. Kishikawa, H. Takezoe, *Phys. Rev. E: Stat., Nonlinear, Soft Matter Phys.* **2005**, *72*, 4.
[15] T. Kato, T. Yasuda, Y. Kamikawa, M. Yoshio, *Chem. Commun.* **2009**, 729.
[16] H. Takezoe, K. Kishikawa, E. Gorecka, *J. Mater. Chem.* **2006**, *16*, 2412.
[17] K. Kishikawa, S. Nakahara, Y. Nishikawa, M. Natsukawa, S. Kohmoto, *Mol. Cryst. Liq. Cryst.* **2009**, *498*, 11.
[18] M. García-Iglesias, B. F. M. de Waal, A. V. Gorbunov, A. R. A. Palmans, M. Kemerink, E. W. Meijer, *J. Am. Chem. Soc.* **2016**, *138*, 6217.
[19] J. C. Roberts, Z. M. Hudson, R. P. Lemieux, *J. Mater. Chem.* **2008**, *18*, 3361.
[20] Y. Funatsu, A. Sonoda, M. Funahashi, *J. Mater. Chem. C* **2015**, *3*, 1982.
[21] R. Ohtani, M. Nakaya, H. Ohmagari, M. Nakamura, K. Ohta, L. F. Lindoy, S. Hayami, *Sci. Rep.* **2015**, *5*, 16606.
[22] S. Inoue, H. Minemawari, J. Tsutsumi, M. Chikamatsu, T. Yamada, S. Horiuchi, M. Tanaka, R. Kumai, M. Yoneya, T. Hasegawa, *Chem. Mater.* **2015**, *27*, 3809.
[23] W. Pisula, Ž. Tomović, C. Simpson, M. Kastler, T. Pakula, K. Müllen, *Chem. Mater.* **2005**, *17*, 4296.
[24] J. Min, Y. N. Luponosov, A. Gerl, M. S. Polinskaya, S. M. Peregudova, P. V. Dmitryakov, A. V. Bakirov, M. A. Shcherbina, S. N. Chvalun, S. Grigorian, N. Kaush-Busies, S. A. Ponomarenko, T. Ameri, C. J. Brabec, *Adv. Energy Mater.* **2014**, *4*, 1301234.
[25] Y. Hirai, H. Monobe, N. Mizoshita, M. Moriyama, K. Hanabusa, Y. Shimizu, T. Kato, *Adv. Funct. Mater.* **2008**, *18*, 1668.
[26] E. O. Arikainen, N. Boden, R. J. Bushby, J. Clements, B. Movaghar, A. Wood, *J. Mater. Chem.* **1995**, *5*, 2161.
[27] F. Kentischer, R. Macdonald, P. Warnick, G. Heppke, *Liq. Cryst.* **1998**, *25*, 341.
[28] K. Kishikawa, S. Nakahara, M. Natsukawa, K. Suzuki, S. Kohmoto, *Mol. Cryst. Liq. Cryst.* **2010**, *516*, 107.
[29] Y. Matsunaga, N. Miyajima, Y. Nakayasu, S. Sakai, M. Yonenaga, *Bull. Chem. Soc. Jpn.* **1988**, *61*, 207.
[30] S. Cantekin, T. F. A. de Greef, A. R. A. Palmans, *Chem. Soc. Rev.* **2012**, *41*, 6125.
[31] M. B. Baker, L. Albertazzi, I. K. Voets, C. M. A. Leenders, A. R. A. Palmans, G. M. Pavan, E. W. Meijer, *Nat. Commun.* **2015**, *6*, 6234.
[32] Y. Yasuda, E. Iishi, H. Inada, Y. Shirota, *Chem. Lett.* **1996**, *25*, 575.
[33] D. Kluge, J. C. Singer, J. W. Neubauer, F. Abraham, H. W. Schmidt, A. Fery, *Small* **2012**, *8*, 2563.
[34] M. Kristiansen, P. Smith, H. Chanzy, C. Baerlocher, V. Gramlich, L. McCusker, T. Weber, P. Pattison, M. Blomenhofer, H. W. Schmidt, *Cryst. Growth Des.* **2009**, *9*, 2556.
[35] A. V. Gorbunov, T. Putzeys, I. Urbanavičiūtė, R. A. J. Janssen, M. Wübbenhorst, R. P. Sijbesma, M. Kemerink, *Phys. Chem. Chem. Phys.* **2016**, *18*, 23663.
[36] C. F. C. Fitié, W. S. C. Roelofs, P. C. M. M. Magusin, M. Wübbenhorst, M. Kemerink, R. P. Sijbesma, *J. Phys. Chem. B* **2012**, *116*, 3928.
[37] R. Q. Albuquerque, A. Timme, R. Kress, J. Senker, H. W. Schmidt, *Chem. – Eur. J.* **2013**, *19*, 1647.
[38] K. K. Bejagam, S. Balasubramanian, *J. Phys. Chem. B* **2015**, *119*, 5738.
[39] K. K. Bejagam, G. Fiorin, M. L. Klein, S. Balasubramanian, *J. Phys. Chem. B* **2014**, *118*, 5218.
[40] K. K. Bejagam, C. Kulkarni, S. J. George, S. Balasubramanian, *Chem. Commun.* **2015**, *51*, 16049.
[41] G. Ayton, G. N. Patey, *Phys. Rev. Lett.* **1996**, *76*, 239.
[42] T. K. Bose, J. Saha, *Phys. Rev. Lett.* **2013**, *110*, 265701.
[43] T. K. Bose, J. Saha, *Phys. Rev. E: Stat., Nonlinear, Soft Matter Phys.* **2014**, *89*, 1.
[44] T. K. Bose, J. Saha, *Phys. Rev. E* **2015**, *92*, 42503.
[45] A. Timme, R. Kress, R. Q. Albuquerque, H. W. Schmidt, *Chem. – Eur. J.* **2012**, *18*, 8329.
[46] P. J. M. Stals, M. M. J. Smulders, R. Martín-Rapún, A. R. A. Palmans, E. W. Meijer, *Chem. – Eur. J.* **2009**, *15*, 2071.
[47] Y. Shishido, H. Anetai, T. Takeda, N. Hoshino, S. I. Noro, T. Nakamura, T. Akutagawa, *J. Phys. Chem. C* **2014**, *118*, 21204.
[48] M. Vopsaroiu, J. Blackburn, M. G. Cain, P. M. Weaver, *Phys. Rev. B* **2010**, *82*, 024109.

[49] C. Kulkarni, S. K. Reddy, S. J. George, S. Balasubramanian, *Chem. Phys. Lett.* **2011**, *515*, 226.
[50] A. V. Gorbunov, X. Meng, I. Urbanaviciute, T. Putzeys, M. Wübbenhorst, R. P. Sijbesma, M. Kemerink, *Phys. Chem. Chem. Phys.* **2017**, *19*, 3192.
[51] X. J. Lou, *J. Appl. Phys.* **2009**, *105*, 094107.
[52] A. Gruverman, H. Tokumoto, A. S. Prakash, S. Aggarwal, B. Yang, *Appl. Phys. Lett.* **1997**, *71*, 3492.
[53] R. R. Mehta, B. D. Silverman, J. T. Jacobs, *J. Appl. Phys.* **1973**, *44*, 3379.
[54] P. Heremans, G. H. Gelinck, R. Müller, K. J. Baeg, D. Y. Kim, Y. Y. Noh, *Chem. Mater.* **2011**, *23*, 341.
[55] A. K. Tagantsev, I. Stolichnov, N. Setter, J. S. Cross, M. Tsukada, *Phys. Rev. B* **2002**, *66*, 214109.
[56] J. Y. Jo, H. S. Han, J.-G. Yoon, T. K. Song, S.-H. Kim, T. W. Noh, *Phys. Rev. Lett.* **2007**, *99*, 267602.
[57] R. C. G. Naber, K. Asadi, P. W. M. Blom, D. M. De Leeuw, B. De Boer, *Adv. Mater.* **2010**, *22*, 933.
[58] D. Zhao, I. Katsouras, M. Li, K. Asadi, J. Tsurumi, G. Glasser, J. Takeya, P. W. M. Blom, D. M. de Leeuw, *Sci. Rep.* **2014**, *4*, 5075.
[59] D. Zhao, I. Katsouras, K. Asadi, P. W. M. Blom, D. M. de Leeuw, *Phys. Rev. B* **2015**, *92*, 1.
[60] U. S. Bhansali, M. A. Khan, H. N. Alshareef, *Microelectron. Eng.* **2013**, *105*, 68.
[61] V. Khikhlovskyi, A. J. J. M. Van Breemen, R. A. J. Janssen, G. H. Gelinck, M. Kemerink, *Org. Electron.* **2016**, *31*, 56.